

Are extreme AGB stars post-common envelope binaries?

F. Dell’Agli¹, E. Marini^{1,2}, F. D’Antona¹, P. Ventura¹, M. A. T. Groenewegen³,
L. Mattsson⁴, D. Kamath⁵, D. A. García–Hernández^{6,7}, M. Tailo⁸

¹INAF, Observatory of Rome, Via Frascati 33, 00077 Monte Porzio Catone (RM), Italy

²Dipartimento di Matematica e Fisica, Università degli Studi Roma Tre, via della Vasca Navale 84, 00100, Roma, Italy

³Koninklijke Sterrenwacht van België, Ringlaan 3, 1180 Brussels, Belgium

⁴Nordita, KTH Royal Institute of Technology and Stockholm University, Roslagstullsbacken 23, SE-106 91 Stockholm, Sweden

⁵Department of Physics and Astronomy, Macquarie University, Sydney, NSW 2109, Australia

⁶Instituto de Astrofísica de Canarias (IAC), E-38205 La Laguna, Tenerife, Spain

⁷Departamento de Astrofísica, Universidad de La Laguna (ULL), E-38206 La Laguna, Tenerife, Spain

⁸Dipartimento di Fisica e Astronomia ‘Galileo Galilei’, Univ. di Padova, Vicolo dell’Osservatorio 3, I-35122 Padova, Italy

24 April 2021

ABSTRACT

Modelling dust formation in single stars evolving through the carbon-star stage of the asymptotic giant branch (AGB) reproduces well the mid-infrared colours and magnitudes of most of the C-rich sources in the Large Magellanic Cloud (LMC), apart from a small subset of extremely red objects (EROs). The analysis of EROs spectral energy distribution suggests the presence of large quantities of dust, which demand gas densities in the outflow significantly higher than expected from theoretical modelling. We propose that binary interaction mechanisms that involve common envelope (CE) evolution could be a possible explanation for these peculiar stars; the CE phase is favoured by the rapid growth of the stellar radius occurring after C/O overcomes unity. Our modelling of the dust provides results consistent with the observations for mass-loss rates $\dot{M} \sim 5 \times 10^{-4} \dot{M}/\text{yr}$, a lower limit to the rapid loss of the envelope experienced in the CE phase. We propose that EROs could possibly hide binaries of orbital periods \sim days and are likely to be responsible for a large fraction of the dust production rate in galaxies.

Key words: stars: AGB and post-AGB – stars: carbon – binaries: general – mass loss – dust – Magellanic Clouds

1 INTRODUCTION

Stars of mass in the $\sim 1 - 8 M_{\odot}$ range evolve through the asymptotic giant branch (AGB) phase. AGB stars experience the third dredge-up (TDU), the inward penetration of the envelope down to regions that previously sited of triple- α nucleosynthesis (Iben 1974). In stars with mass $< 4 M_{\odot}$ repeated TDU events cause a gradual rise in the surface carbon; if the number of carbon nuclei exceeds that of oxygen, the star becomes a carbon star (C-star). During the AGB evolution the stars are exposed to strong mass loss via cold and dense stellar wind, suitable for the condensation of dust.

A thorough comprehension of the evolution of C-stars is fundamental to understand still poorly known physical mechanisms that take place in stellar interiors, primarily convection and mixing. Furthermore, C-stars are the most efficient sources of carbon gas in the interstellar medium (ISM; Romano et al. (2020)). Furthermore, while in solar-metallicity environments the dust return to the ISM is dominated by O-rich stars (Javadi et al. 2013), recent studies shown that in lower-metallicity environments the dust production rate (DPR) is dominated by carbon dust (e.g. Boyer et al. 2012; Schneider et al. 2014; Dell’Agli et al. 2016, 2019), with a relevant contribution from the most obscured stars.

The existence of stars with extremely red mid-IR colours (EROs) in the LMC was discovered by Gruendl et al. (2008), who used Spitzer IRAC and MIPS photometry and IRS follow-up spectroscopy to

identify these objects as extreme C-stars. Sloan et al. (2016) and Groenewegen & Sloan (2018) discussed the peculiarity of these sources and the possible implications related to the large IR emission. Dell’Agli et al. (2015) and Nanni et al. (2019) studied the LMC population of evolved stars following an approach based on the results from stellar evolution and dust formation modelling, but could not explain the whole set of photometric and spectroscopic data of the stars in the Gruendl et al. (2008) sample.

In this work we reconsider the EROs from the Gruendl et al. (2008) sample in the attempt of modelling the detailed morphology of the spectral energy distribution (SED), based on IRS data. We discuss the possibility that their unusual IR excess is connected with the presence of large amounts of dust in their surroundings, due to the common envelope (CE) evolution occurring during the C-star phase of the AGB. We consider binary systems in the orbital period range ~ 2.5 -15 yr, where the primary component, an AGB C-star, fills the Roche lobe (RL) first, begins to lose mass and starts a phase of rapid expansion, which further enhances the mass loss rate, a phenomenon that proceeds on a dynamical timescale (Paczynski 1976).

This investigation can pose important clues to understand the overall dust production efficiency by evolved stars in galaxies.

2 STELLAR EVOLUTION AND DUST FORMATION MODELLING

We calculated evolutionary sequences of $Z = 0.008$ stars with initial mass in the $1 - 3.5 M_{\odot}$ range. Stars with mass $M < 1 M_{\odot}$ are not considered because they do not become C-stars, as well as $M \geq 4 M_{\odot}$, because they experience hot bottom burning, which destroys the surface carbon and inhibits the C-star stage (Ventura et al. 2014).

The evolutionary sequences were calculated using the ATON code for stellar evolution (Ventura et al. 1998). Convection, mass loss, opacities are described as in Ventura et al. (2014). We modelled dust formation in the winds of AGB stars following the schematisation proposed by Ferrarotti & Gail (2006). Dust particles are assumed to form and grow in the outflow, which expands isotropically from the photosphere of the star. Dust growth is governed by the rate with which gas molecules collide with pre-existing seed particles, in turn connected to the molecules number density and thermal velocity. Dust formation is assumed to begin at the point in the outflow where the growth rate exceeds the vapourization rate, in turn related to the difference between the formation enthalpies of the solid compound and the individual gaseous reactants. All the relevant equations can be found in Ventura et al. (2012).

The dust formation modelling is applied to some points during each inter-pulse and thermal pulse (TP) phase, chosen to properly follow the variation in the evolutionary properties of each star. This allows to determine the evolution of the dust composition and of τ_{10} , the optical depth at $\lambda = 10 \mu\text{m}$. The outcomes of the star+dust modelling were used as input for the radiation transport code DUSTY (Nenkova et al. 1999), to build a sequence of synthetic SEDs, which allow to simulate the evolution of the (circum)stellar spectrum. The convolution with the transmission curves of various filters allows to compute evolutionary tracks in the observational planes based on different photometric systems (black tracks in Fig. 1).

3 THE EVOLUTIONARY PATTERN OF CARBON STARS

The left panel of Fig. 1 shows the evolution of AGB star models in the $\tau_{10} - L$ plane. The increase in τ_{10} is due to the gradual rise in the surface carbon and the consequent expansion of the external regions (Ventura & Marigo 2009). These factors lead to a more efficient dust formation, owing to the higher availability of carbon molecules and to the cooler temperatures in the envelope, which favour condensation with respect to vaporisation (Ferrarotti & Gail 2006).

In the central panel of Fig. 1 we show the evolutionary tracks in the $([5.8]-[8.0], [8.0])$ colour-magnitude diagram constructed on the basis of the IRAC filters of the *Spitzer Space Telescope*. The right panel of Fig. 1 shows the evolutionary tracks in the $([F770W]-[F1800W], [F1800W])$ diagram, where [F770W] and [F1800W] are the magnitudes obtained by convolving the synthetic SED with the transmission curves of two mid-IR filters of the MIRI camera, mounted onboard the upcoming *James Webb Space Telescope (JWST)*.

3.1 The extreme carbon star stage

Grey points and red pentagons in Fig. 1 refer to the LMC C-stars observed by *Spitzer*, in the area of the sky covered by the SAGE survey (Meixner et al. 2006). Jones et al. (2017) calculated the expected [F770W] and [F1800W] of these objects, via convolution of the IRS spectra with the MIRI transmission curves.

Here we focus on the stars characterised by large IR excess, indicated with red symbols in Fig. 1, that involve the extreme stars

from Gruendl et al. (2008) and SSID 9, which shares similar characteristics. The appropriate combination of τ_{10} and dust composition allows to fit the observations, by reproducing all the major features in the spectra. The position of the red points in the left panel of Fig. 1 was determined by adopting this method. Two examples of the SED fitting results are shown in the left and central panel of Fig. 2 for the sources SSID 4171 and 4489. The main properties derived for the EROs are summarised in Table 1.

The optical depths of these stars are significantly higher than the theoretical expectations. Some consistency is found only for the brightest extreme stars, whose luminosity and τ_{10} are similar to those of the last point of the track of the $3 M_{\odot}$ star. In the colour-magnitude plane, the evolutionary tracks reproduce the position of most evolved LMC stars in the sample, with the exception of the EROs.

The method used to determine the optical depths of the model described in Sect. 2 has some limitations. The stationary wind neglects the effects of pulsation (Höfner & Olofsson 2018), which might potentially eject dense gas clouds into cool regions of the circumstellar envelope, where dust formation would be favoured. Furthermore, no gas-dust drift is considered, which might lead to an underestimation of the dust formed (Sandin & Mattsson 2020).

Despite these uncertainties, we believe that there is not much room to significantly widen the extension of the evolutionary tracks in Fig. 1. The key factor for dust formation in the outflow during a given evolutionary stage is the mass-loss rate \dot{M} , which determines the density of the wind and thus of the molecular species available to condensation. The terminal points of the sequences in Fig. 1 are characterised by $\dot{M} \sim 1 - 2 \times 10^{-4} M_{\odot}/\text{yr}$, calculated based on Wachter et al. (2002), which might overestimate the \dot{M} of C-stars (Bladh et al. 2019). Higher \dot{M} are thus difficult to justify in the present context. The discrepancy between modelling and observations is particularly relevant for the three faintest stars, whose luminosities indicate $\sim 1 - 1.5 M_{\odot}$ progenitors. These stars reach the C-star stage during the final AGB phases, with a surface C/O below 1.5: the corresponding carbon excess with respect to oxygen is likely not sufficient to drive a dust-driven wind (Bladh et al. 2019).

3.2 The effects of enhanced mass-loss

We tested the effects on dust production if we increase the mass loss rate at an earlier evolutionary stage, namely soon after $C/O > 1$. We resumed the computations of the $1.1, 2.5$ and $3 M_{\odot}$ models, from the stages indicated by the blue arrows in the left panel of Fig. 3, after the jump in the radius following a TDU episode. We kept the mass loss rate at $\dot{M} = 5 \times 10^{-4} M_{\odot}/\text{yr}$, a first order approximation to the situation encountered in the CE of a binary system during the evolution (see next Section), where an envelope of $\sim 1 M_{\odot}$ can be lost even in 10 yr (Chamandy et al. 2020) and matter will transfer out of the Lagrangian points until it is dispersed. For the $2.5 M_{\odot}$ model star we considered an additional case, where the enhanced mass loss is assumed from a later stage (green arrow in Fig. 3). We model dust formation as in the spherical, single star evolution (SSE), although the time-scale of the events is so short that the details of the nucleation processes which lead to the formation of the seed particles on which dust grains grow might be different. Besides, neglecting the non-spherical structure of the outflow might lead to an overestimation of the \dot{M} required to account for the observed IR emission (Sloan et al. 2016; Wiegert et al. 2020). These points deserve further investigation in the future. Despite this, CE evolution appears as a good candidate to justify the dust emission of these EROs, because the higher mass-loss favoured by the CE interaction increases the density of gaseous molecules available to form dust,

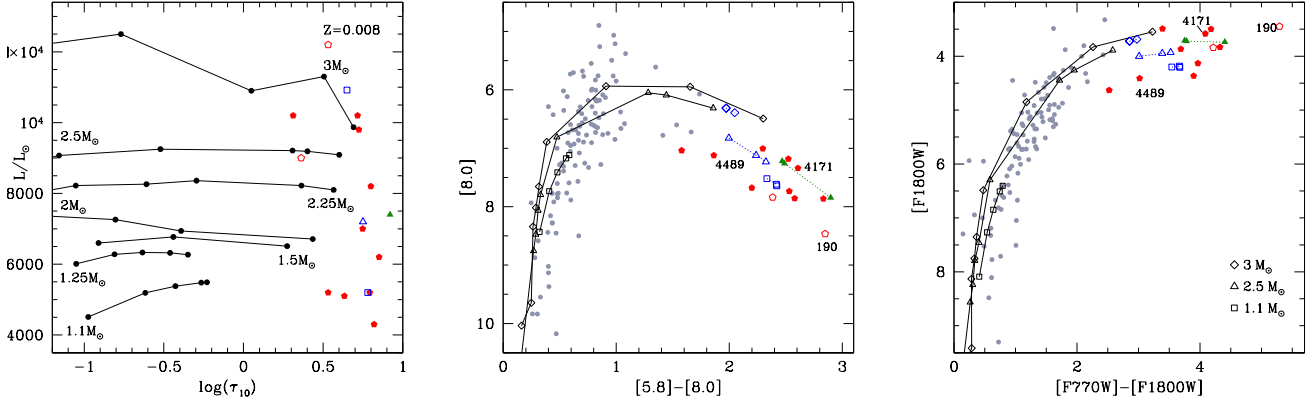


Figure 1. Left: The evolution of stars of different mass in the $\tau_{10} - L/L_{\odot}$ plane. Red pentagons indicate the optical depths and magnitudes of the EROs sources, obtained by SED fitting. Open blue points refer to the evolution of $1.1 M_{\odot}$ (square), $2.5 M_{\odot}$ (triangle) and $3.0 M_{\odot}$ (diamond) when assuming an enhanced mass-loss rate immediately after the beginning of the C-star phase or in a more advanced stage (full green triangles). The evolutionary tracks (black solid lines), LMC C-stars from the SAGE-Spec database (grey points) and EROs sources (red pentagons) in the colour-magnitude ($[5.8]-[8.0]$, $[8.0]$) and $([F770W]-[F1800W]$, $[F1800W])$ planes, respectively. The evolutionary points found when assuming an enhanced mass-loss rate (blue points with dashed lines), simulating the CE phase, are reported in both panels. Open pentagons refer to SSID 190 and SSID 125.

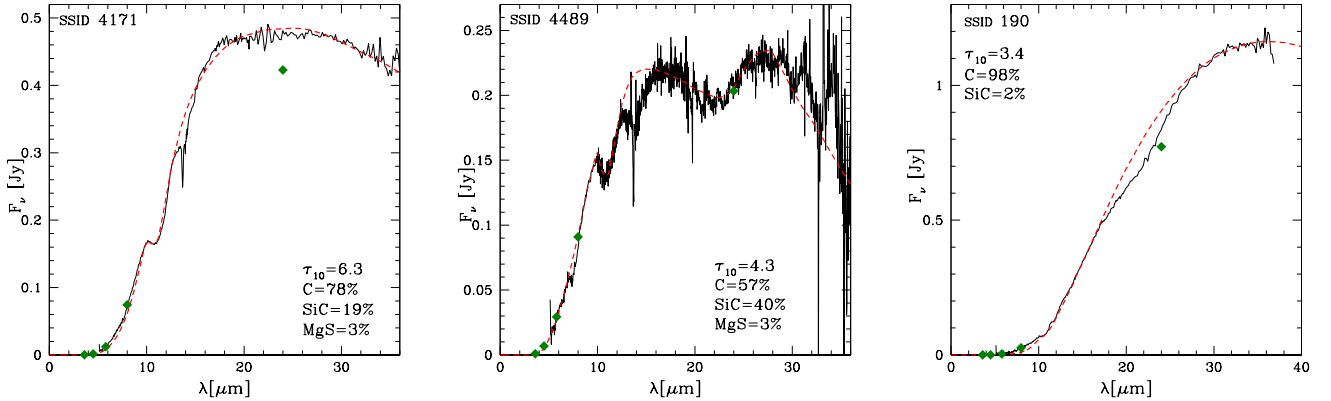


Figure 2. IRS SED of SSID 4171 (left panel), SSID 4489 (centre) and SSID 190 (right) indicated with black lines and the best fit (red lines), obtained with the optical depth and the dust mineralogy reported in the figures. Photometry from IRAC and MIPS is indicated with green diamonds.

Table 1. Summary of the interpretation of the stars discussed in this work: Spitzer and IRAC/ERO name, coordinates, luminosity, optical depth, percentages of the different dust species (in order: solid carbon, silicon carbide, magnesium sulphide, graphite), initial mass and age.

SSID	IRAS/ERO name	RA (deg)	DEC (deg)	L/L_{\odot}	τ_{10}	%(C)	%(SiC)	%(MgS)	%(graph)	$M_{\text{init}}/M_{\odot}$	Age (Gyr)
4185	IRAS 05042-6827	76.0233	-68.3945	5200	6.2	67	25	2	6	1.1 – 1.2	5.0 – 7.0
4299	IRAS 05187-7033	79.5488	-70.5075	9800	5.3	79	0	0	21	2.5 – 3.0	0.4 – 0.6
4308	IRAS 05191-6936	79.7016	-69.5596	7000	5.6	64	22	2	12	2.0 – 2.5	0.6 – 1.0
4415	IRAS 05260-7010	81.4193	-70.1409	4700	6.6	68	18	2	12	1.1 – 1.2	5.0 – 7.0
4171	ERO 0502315	75.6312	-68.0934	8200	6.3	68	19	3	10	2.0 – 2.5	0.6 – 1.0
4489	IRAS 05305-7251	82.4079	-72.8314	5100	4.3	53	40	3	4	1.1 – 1.2	5.0 – 7.0
4781	IRAS 05509-6956	87.6091	-69.9342	10200	5.2	68	27	3	2	2.5 – 3.0	0.4 – 0.6
9	IRAS 04518-6852	72.9192	-68.7930	5200	3.4	75	14	5	6	1.1 – 1.2	5.0 – 7.0
65	IRAS 05133-6937	78.2576	-69.5642	6200	7.1	76	20	2	2	1.5 – 2.0	1.0 – 2.0
125	IRAS 05315-7145	82.6853	-71.7167	9000	2.3	62	14	2	24	2.0 – 2.5	0.6 – 1.0
190	IRAS 05495-7034	87.2504	-70.5562	12200	3.4	83	2	2	15	3.0 – 3.5	0.3 – 0.4

consistently with the study by [Glanz & Perets \(2018\)](#), who showed that efficient dust production takes place following CE interaction.

The evolution of the tracks in Fig. 1 during the enhanced mass loss phase (blue and green points) reproduces the observed locations of EROs. The redder objects are better reproduced by the models where the enhanced mass loss is started later (green triangles), because the higher surface carbon favours a larger dust production. In the $3 M_{\odot}$ case use of the higher \dot{M} does not change τ_{10} in a meaningful way. This is because the surface carbon mass fraction at the point when we assumed the large \dot{M} is 3 times smaller than during the final phases of the "standard" case, corresponding to the reddest point of the evolutionary track; this effect counterbalances the higher \dot{M} . This is also the reason why the dust yields of $2.5 - 3 M_{\odot}$ stars are unchanged with respect to the SSE (see Fig. 10 in [Ventura et al. \(2014\)](#)). Conversely, in $1.1 M_{\odot}$ stars, in which the CE phase begins towards the end of the AGB, the C dust produced is two times higher.

The spectra of SSID 125 and 190 (see Fig. 2 for the latter source) show up dissimilarities with the other sources discussed here. From the interpretation of their SED we find dust temperatures ~ 300 K, much cooler than the other stars, and optical depths $\tau_{10} \sim 2 - 3$, the lowest reported in Table 1. These results might indicate that the primary has started the post-AGB evolution, with the dusty region moving away from the central star ([Groenewegen & Sloan 2018](#)).

4 COMMON ENVELOPE EVOLUTION: HOW TO REACH HIGH MASS LOSS AT AN EARLIER PHASE

In the previous Section we describe how the large IR emissions can be obtained via the occurrence of very large mass loss rates earlier during the AGB phase, even as soon as $C/O > 1$. In this Section, we explore a plausible situation which may produce this effect.

In fact, if the AGB star is in a binary system, its evolution may be affected by the presence of the companion. The basic subdivision of binary interaction made by [Paczynski \(1971\)](#) classifies as "Case C" the evolution of a binary when the primary component (the most massive star) fills its RL and begins mass exchange during the AGB phase. As a reaction to mass loss, the stellar radius of a donor having a deep convective envelope increases, while the binary separation decreases when mass is transferred to the less massive companion. Thus, mass is lost from the AGB star at very high rates, while the cores of the two components spiral towards each other in a CE phase ([Paczynski 1976](#)). Note that pre-CE binary interaction has generally negligible consequences for the CE event. The binary interaction occurs when the systems have orbital period P_{orb} of years, but the orbital angular momentum transfer from the inner cores to the outer layers is so large that the final period may be in the range of days or even hours (e.g. [Willems & Kolb 2004](#)), and the shortest P_{orb} post-CE systems will be the progenitors of cataclysmic binaries (CBs), in which a low mass quasi-main sequence star (the previous secondary star) is now the component filling the RL and transferring mass to the (former primary) white dwarf (WD). The existence of binary nuclei of planetary nebulae (see e.g. [Jones & Boffin 2017](#)) has confirmed the scheme, and the properties of the remnant post-CE binary and CB population have been explored in several population synthesis models (e.g. [Willems & Kolb 2004](#))¹.

Full consideration of the effect of the wind mass loss from the

AGB star and of the structure details of the AGB envelopes and the effect of TPs may be important to understand which systems evolve into stable case C evolution ([Pastetter & Ritter 1989](#)) and to outline the precise evolutionary boundaries for which the present proposal is feasible. However, for this study we are interested mainly in those systems which: 1) suffer unavoidable CE evolution; 2) when they are already C-stars; 3) where the CE allows to meet the required dust density production which is not allowed during the SSE.

4.1 The stellar radius evolution

The main parameter determining whether the AGB star will evolve into RL contact is the evolution of the stellar radius. In our case, the current binary separation (or P_{orb}) must be such that mass exchange did not begin during the red giant branch (RGB) phase. We examine three representative masses: 1.1 , 2.5 and $3.0 M_{\odot}$. The left panel of Fig. 3 shows the radius evolution as a function of the current mass for the three cases. Note that the SSE includes mass loss by stellar wind, so the mass is a proxy of the advancement of the time.

While the 2.5 and $3 M_{\odot}$ cases have relatively small radii at the onset of central helium burning (29 and $34 R_{\odot}$), the $1.1 M_{\odot}$ undergoes helium flash at a radius $R = 124 R_{\odot}$; this value is smaller than during the first TPs and ~ 2.5 times lower than during the C-star phase. We consider binary systems exceeding the $P_{\text{orb}} \sim 1$ yr, which would have produced mass exchange during the RGB.

As shown in Fig. 3, the radius during the SSE begins increasing with a steep derivative for $C/O \sim 1.5$, owing to the increase in the surface molecular opacities (see Sect. 3). Thus, the case in which the AGB star is the primary in a detached binary, filling the RL as C-star, occurs for a wide range of P_{orb} . In the right panel of Fig. 3 is shown P_{orb} for a (non interacting) binary in which the primary has the AGB mass, with a radius equal to the RL radius (computed following eq. 2 and 3 in [Eggleton 1983](#), see left panel of Fig. 3), and the companion has a mass of $0.6 M_{\odot}$ or $0.8 M_{\odot}$. P_{orb} in Fig. 3 is thus the "initial" possible period of a binary at the moment it can interact with the companion. It is self-evident that, if the primary has not filled the RL in previous evolutionary phases, there is a huge range of initial periods ($\sim 2.5 - 15$ yrs, the precise range depending on the evolving mass) during which this may happen, giving origin to the high mass loss which favours the production of dust.

5 DISCUSSION AND CONCLUSIONS

We propose that the EROs can be interpreted as the result of the evolution of binaries of periods $\sim 2.5 - 15$ yr (see Fig. 3), in which the primary is an AGB star of mass $1.1 - 3.0 M_{\odot}$ evolving through the C-star phase, and the companion is a star of mass low enough that the mass transfer is unstable. $M > 1.2 M_{\odot}$ companion stars cannot be considered, as they expand as a reaction to mass accretion, and the system would follow a different route with respect to the one proposed here. The binary system evolves through a CE phase and ends up as a pre-cataclysmic binary of periods of the order of days. We simulate the evolution of the AGB by assuming a high constant mass loss rate, and computing the dust evolution. This work provides proof of concept for the hypothesis that the parameters of the CE evolution are not particularly tight, and that the resulting dust is indeed of density high enough to produce the colors of the EROs. Computation of

binaries ($\sim 0.6 M_{\odot}$) ([Zorotovic, Schreiber, & Gänsicke 2011](#)), which is also the typical WD mass remnant of our proposed evolution.

¹ Not all post-CE binaries evolve into the interacting stage, and research is now ongoing (e.g. [Wijnen, Zorotovic, & Schreiber 2015](#)) to understand why the average mass of the WD components of CBs are much larger ($\sim 0.8 M_{\odot}$) than the average mass of carbon-oxygen white dwarfs remnants of post-CE

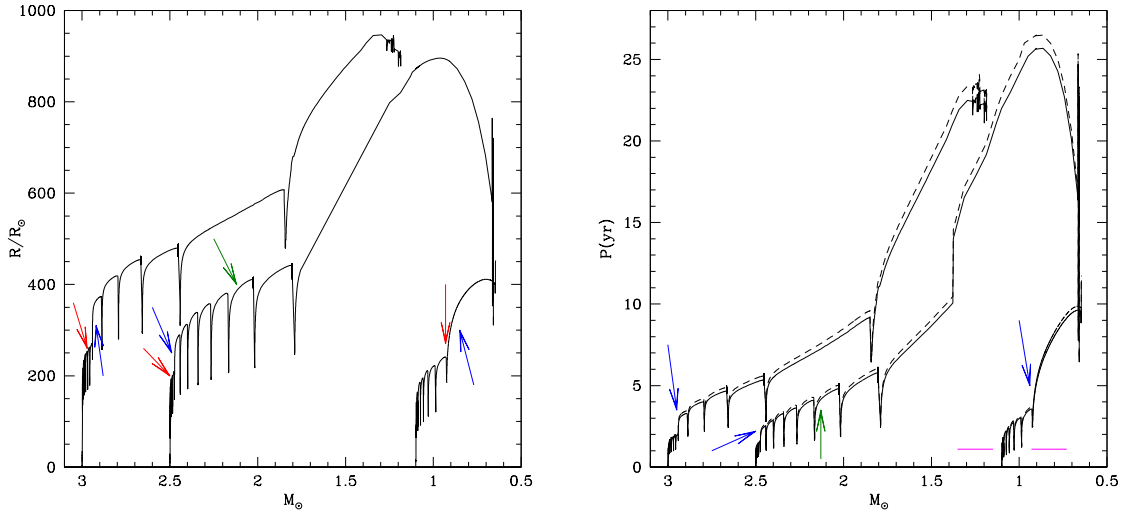


Figure 3. Left: variation of the radius of initial mass models $1.1 M_{\odot}$, $2.5 M_{\odot}$ and $3 M_{\odot}$, as a function of the current mass of the star. Arrows mark the beginning of the C-star phase (red) and when the star rapidly expands (blue and green), due to the surface carbon enrichment. Right: orbital period evolution, intended as the initial period of a binary in which the AGB fills the RL at each point of mass along its SSE. Solid and dashed lines refer to the cases in which the companion mass is $0.6 M_{\odot}$ and $0.8 M_{\odot}$, respectively. If contact occurs at the indicated points (blue or green arrows), a CE evolution and rapid shrinking of the period is expected. Magenta line marks the period of the system if the contact would occur when the $1.1 M_{\odot}$ star is at the tip of the RGB.

populations synthesis may be useful to constrain the number of such systems expected in the Galaxy; these stars may be more efficient dust producers than the much more numerous AGBs evolving as single stars (e.g. Boyer et al. 2012). The fact that the EROs observed so far are all C-stars can be explained by the constraints given above on the mass of the companion: systems with a $4 - 6 M_{\odot}$ primary would experience a CE evolution only if the mass ratio is above 4-5, which renders these events rather rare. We conclude this work with a plea to look for signs of carbon dust, having survived the CE ejection, in post-CE systems where the AGB descendant has $0.55 \leq M/M_{\odot} \leq 0.7$, typical core mass of C-stars.

ACKNOWLEDGEMENTS

We would like to thank the referee Dr. J. Th. van Loon for his useful suggestions. DAGH acknowledges support from the State Research Agency (AEI) of the Spanish Ministry of Science, Innovation and Universities (MCIU) and the European Regional Development Fund (FEDER) under grant AYA2017-88254-P. DK acknowledges the support of the Australian Research Council (ARC) Decra grant (95213534).

DATA AVAILABILITY

The data underlying this article will be shared on reasonable request to the corresponding author.

REFERENCES

Bladh S., Eriksson K., Marigo P., Liljegren S., Aringer B. 2019, *A&A*, 623, A119
 Boyer M. L., Srinivasan S., Riebel D., McDonald I. et al. 2012, *ApJ*, 748, 40

Chamandy L., Blackman E. G., Frank A., Carroll-Nellenback J., Tu Y., 2020, *MNRAS*, 495, 4028
 Dell’Agli F., Ventura P., Schneider R., Di Criscienzo M., García-Hernández D. A., Rossi C., Brocato E. 2015, *MNRAS*, 447, 2992
 Dell’Agli F., Di Criscienzo M., Boyer M. L., García-Hernández D. A. 2016, *MNRAS*, 460, 4230
 Dell’Agli F., Di Criscienzo M., García-Hernández D. A., Ventura P., Limongi M., Marini E., Jones O. C. 2019, *MNRAS*, 482, 4733
 Eggleton P. P., 1983, *ApJ*, 268, 368
 Ferrarotti A. S., Gail H.-P. 2006, *A&A*, 447, 553
 Glanz H., Perets H. B. 2018, *MNRAS*, 478, 12
 Groenewegen, M. A. T., & Sloan, G. C. 2018, *A&A*, 609, A114
 Gruendl R. A., Chu Y.-H., Seale J. P., et al. 2008, *ApJ*, 688, L9
 Iben I. Jr. 1974, *ARA&A*, 12, 215
 Höfner S., Olofsson H., 2018, *A&ARv*, 26, 92
 Javadi A., van Loon J. T., Khosroshahi H., Mirtorabi M. T., 2013, *MNRAS*, 432, 2824
 Jones D., Boffin H. M. J., 2017, *NatAs*, 1, 0117
 Jones O. C., Meixner M., Justtanont K., Glasse A. 2017, *ApJ*, 841, 15
 Mattsson L., 2016, *Mem. SAI*, 87, 249
 Meixner M., Gordon K. D., Indebetouw R., et al. 2006, *AJ*, 132, 2268
 Nanni A., Groenewegen M. A. T., Aringer B. et al. 2019, *MNRAS*, 487, 502
 Nenkova, M., Ivezić, Z., & Elitzur, M. 1999, *Thermal Emission Spectroscopy and Analysis of Dust, Disks, and Regoliths*, 20
 Paczyński B., 1971, *ARA&A*, 9, 183
 Paczynski B., 1976, *IAUS*, 73, 75
 Pastetter L., Ritter H., 1989, *A&A*, 214, 186
 Romano D., Franchini M., Grisoni V., Spitoni E., Matteucci F., Morossi C. 2020, *A&A*, 639, A37
 Sandin C., Mattsson L., 2020, *MNRAS*, 499, 1531.
 Schneider R., Valiante R., Ventura P., Dell’Agli F., Di Criscienzo M., Hirashita H., Kemper F. 2014, *MNRAS*, 442, 1440
 Sloan G. C., Kraemer K. E., McDonald I., et al. 2016, *ApJ*, 826, 44
 Ventura P., Zeppieri A., Mazzitelli I., D’Antona F. 1998, *A&A*, 334, 953
 Ventura P., Marigo P. 2009, *MNRAS*, 399, L54
 Ventura P., Di Criscienzo M., Schneider R., et al. 2012, *MNRAS*, 420, 1442
 Ventura P., Dell’Agli F., Schneider R., et al. 2014, *MNRAS*, 439, 977
 Wachter A., Schröder K. P., Winters J. M., Arndt T. U., Sedlmayr E. 2002,

A&A, 384, 452

Wiegert J., Groenewegen M. A. T., Jorissen A., Decin L., Danilovich T., 2020,
arXiv, arXiv:2008.11525

Wijnen T. P. G., Zorotovic M., Schreiber M. R., 2015, A&A, 577, A143

Willems B., Kolb U., 2004, A&A, 419, 1057

Zorotovic M., Schreiber M. R., Gänsicke B. T., 2011, A&A, 536, A42

This paper has been typeset from a \TeX/L\AA\TeX file prepared by the author.